






**Structural sensitivity of the spin Hall magnetoresistance in antiferromagnetic thin films**Andrew Ross <sup>1,2</sup>, Romain Lebrun <sup>1,\*</sup>, Camilo Ulloa,<sup>3</sup> Daniel A. Grave,<sup>4</sup> Asaf Kay,<sup>4</sup> Lorenzo Baldrati <sup>1</sup>, Florian Kronast,<sup>5</sup> Sergio Valencia <sup>5</sup>, Avner Rothschild,<sup>4</sup> and Mathias Kläui <sup>1,2,6</sup><sup>1</sup>*Institut für Physik, Johannes Gutenberg-Universität Mainz, D-55099 Mainz, Germany*<sup>2</sup>*Graduate School of Excellence Materials Science in Mainz (MAINZ), Staudingerweg 9, D-55128 Mainz, Germany*<sup>3</sup>*Institute for Theoretical Physics, Utrecht University, Princetonplein 5, 3584 CC Utrecht, The Netherlands*<sup>4</sup>*Department of Materials Science and Engineering, Technion-Israel Institute of Technology, Haifa 32000, Israel*<sup>5</sup>*Helmholtz-Zentrum Berlin für Materialien und Energie, Albert-Einstein-Strasse 15, D-12489 Berlin, Germany*<sup>6</sup>*Center for Quantum Spintronics, Department of Physics, Norwegian University of Science and Technology, Trondheim, Norway*

(Received 9 May 2020; revised 14 July 2020; accepted 19 August 2020; published 10 September 2020)

Reading the magnetic state of antiferromagnetic (AFM) thin films is key for AFM spintronic devices. We investigate the underlying physics behind the spin Hall magnetoresistance (SMR) of bilayers of platinum and insulating AFM hematite ( $\alpha$ -Fe<sub>2</sub>O<sub>3</sub>) and find an SMR efficiency of up to 0.1%, comparable to ferromagnetic-based structures. To understand the observed complex SMR field dependence, we analyze the effect of misalignments of the magnetic axis that arise during growth of thin films, by electrical measurements and direct magnetic imaging, and find that a small deviation can result in significant signatures in the SMR response. This highlights the care that must be taken when interpreting SMR measurements on AFM spin textures.

DOI: [10.1103/PhysRevB.102.094415](https://doi.org/10.1103/PhysRevB.102.094415)**I. INTRODUCTION**

With spin dynamics in the terahertz regime and a robustness to external perturbations from magnetic fields, antiferromagnetic spintronics seeks to make use of this exciting class of materials for future spintronic devices [1,2]. A pure spin current can be generated in insulating antiferromagnets (AFMI) by several means [3–6]. However, regardless of the excitation mechanism, the detection of such a pure spin current relies on the inverse spin Hall effect in a heavy metal (HM) layer in contact with the AFMI layer. For spin Hall magnetoresistance (SMR), a charge current  $J_C$  flowing in the HM leads to a transverse spin current that flows towards the AFMI/HM interface where it is either absorbed or reflected by the AFMI. This then leads to a modulation of the resistance of the HM as the angle between  $J_C$  and the magnetic order is changed. One can thus theoretically determine the orientation of the antiferromagnetic order parameter, the Néel vector  $\mathbf{n}$ , for both collinear [7–9] and some noncollinear [10] magnetic structures by means of electrical measurements without the need for complex synchrotron-based measurements [11]. There have however been conflicting reports about SMR measurements in antiferromagnets, exhibiting so-called positive SMR [12,13] and negative SMR [7,8] on AFMs as well as the role of the antiferromagnetic symmetry and the interface quality.

While the SMR is expected to depend on the orientation of  $\mathbf{n}$ , significant parasitic contributions can arise from

both ordinary magnetoresistance (OMR) [7,14] and the net magnetic moment of thin-film canted antiferromagnets [13] and ferrimagnets [10]. The SMR has also been investigated in Cr<sub>2</sub>O<sub>3</sub>, which has a locally uncompensated interface that has no noticeable impact on the angular-dependent SMR signals [15,16]. On the theory side, AFMs have been largely treated analogously to ferromagnets although a ferromagnetic interface is uncompensated, leading to real and imaginary components of the spin-mixing conductance [17].

In this paper, we make use of the insulating antiferromagnet hematite,  $\alpha$ -Fe<sub>2</sub>O<sub>3</sub>, which exhibits a phase transition from an easy-plane antiferromagnet (AFM) to an easy-axis (EA) AFM, known as the Morin transition at  $T_M$  [18]. We study the SMR for different antiferromagnetic symmetries without changing the interface by varying the temperature at which the SMR is recorded, finding distinctly different SMR behaviors. Below  $T_M$ , the shape of the SMR cannot be explained using conventional SMR theory. Taking into account the interfacial symmetry then proves critical in the spin transmission. In particular, for our growth direction, the out-of-plane strain on the crystal lattice leads to a small but finite deviation of the magnetic axis from the film normal, as we confirm from direct magnetic imaging. This deviation then heavily influences the resulting SMR signal of easy-axis antiferromagnets highlighting that great care must be taken when analyzing AFM-SMR responses.

**II. MAIN TEXT**

In order to investigate the SMR, epitaxial (0001)-oriented 100-nm thin films of hematite were deposited on likewise orientated sapphire (Al<sub>2</sub>O<sub>3</sub>) via pulsed-laser deposition from a stoichiometric Fe<sub>2</sub>O<sub>3</sub> target at 800 °C [11,19]. Hall bars

\*Present address: Unité Mixte de Physique CNRS, Thales, University Paris-Sud, Université Paris-Saclay, Palaiseau 91767, France.

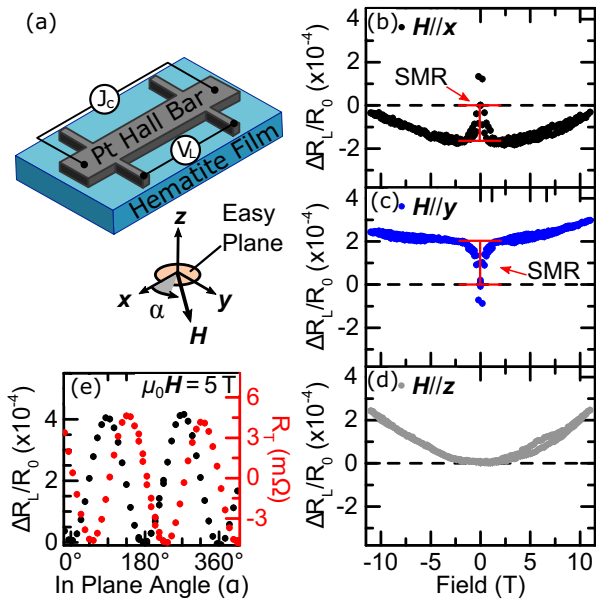


FIG. 1. (a) Schematic of the measurement geometry employed of a Pt Hall bar atop hematite films. The charge current and longitudinal voltage contacts are indicated. The sample  $xy$  plane is the antiferromagnetic easy plane (indicated in orange) above the Morin transition temperature. Normalized longitudinal resistance ( $\Delta R_L = R_L - R_0$ , where  $R_0$  is the zero-field resistance) of a Pt Hall bar atop (0001)-orientated hematite at 300 K in the easy-plane antiferromagnetic phase. The resistance is measured as a function of the magnetic field applied along the (b)  $x$  axis, (c)  $y$  axis, and (d)  $z$  axis. (e) Normalized longitudinal (black) and transverse (red) resistance for an in-plane rotation of the magnetic field  $\mu_0 H = 5$  T ( $\Delta R_L = R_L - R_{\alpha=0^\circ}$ ). Error bars, where visible, represent the standard deviation of the measurement points.

were defined by electron-beam lithography and the subsequent deposition of 7-nm platinum by DC sputtering without additional interfacial treatments. We do not perform additional interfacial treatments due to the propensity of transition-metal oxides to restructure under etching [20]. In the case of hematite, this could lead to a transformation into other (potentially ferrimagnetic) iron oxides [21]. By making use of magnetic dichroism, we do not observe any evidence of such ferrimagnetic oxides at the interface (see Supplemental Material [22]). A charge current  $J_C$  is passed through the Pt Hall bar along the  $x$  axis indicated in Fig. 1(a) which produces a spin accumulation  $\mu_s$  at the interface, polarized along  $y$  while a longitudinal voltage  $V_L$  is detected, from which we calculate a resistance  $R_L$ .

We first investigate the SMR response at room temperature calculated as the change in resistance with respect to the zero-field resistance, normalized to the zero-field resistance ( $\Delta R_L/R_0$ ). At this temperature the  $xy$  plane is the antiferromagnetic easy plane. Like orthoferrites [23], hematite has an antisymmetric exchange interaction (DMI) directed along the (0001) direction that leads to a canting of  $\mathbf{n}$  [24], generating a net magnetic moment  $\mathbf{m} \perp \mathbf{n}$  [18,25], where the role  $\mathbf{m}$  plays in the SMR is currently unclear [10,13,26]. In the absence of a magnetic field  $\mathbf{H}$ ,  $\mathbf{n}$  demonstrates a threefold degeneracy

that leads to an observable magnetic domain structure [27–29] (See also Supplemental Material [22] where we also present spin structures that have the topology of an antiferromagnetic antiskyrmion).  $\mathbf{H}$  applied within the easy plane, parallel ( $\mathbf{H} // x$ ) or perpendicular ( $\mathbf{H} // y$ ) to  $J_C$ , will break this degeneracy and  $\mathbf{n}$  will rotate to lie perpendicular to  $\mathbf{H}$ . The strength of the in-plane anisotropy defines a critical field  $H_{MD}$  required to produce this complete rotation [7,30]. Indeed, for  $\mathbf{H} // x$  we observe initially a decrease of  $R_L$  up to  $H_{MD} = 0.6$  T [Fig. 1(b)]. At  $|\mathbf{H}| > H_{MD}$  the magnetic signal should then saturate, given that AFM-SMR is dependent on the  $y$  component of  $\mathbf{n}$ , i.e.,  $n_y$  [7,8,26,30,31]. However, we observe a sustained increase with increasing magnetic field. If  $\mathbf{H}$  is now directed along  $y$  [Fig. 1(c)] there is a steep increase of  $R_L$  that plateaus at the same field value  $H_{MD}$  as before. Above  $H_{MD}$  there is again a parabolic background. The decrease (increase) of the SMR is related to the change between the zero- and finite field orientations of  $\mathbf{n}$  and  $\mu_s$  where for  $\mathbf{H} // x$ , the final state is  $\mathbf{n} // \mu_s$  (for  $\mathbf{H} // y$ , the final state is  $\mathbf{n} \perp \mu_s$ ) and  $n_y$  increases (decreases) [26,31].

When the magnetic field is applied out of the plane, along  $z$ ,  $\mathbf{n}$  is already perpendicular to  $\mathbf{H}$  and there is no preferred orientation of  $\mathbf{n}$  within the plane. There is however a parabolic change of  $R_L$  with magnetic field [Fig. 1(d)]. This parabolic increase in resistance, present in all field directions on top of the magnetic contributions, possibly stems from the ordinary magnetoresistance of the Pt itself and is unrelated to  $\mathbf{n}$  [7,14,32]. We note that the experimental curve measured in Fig. 1(a) deviates for high magnetic fields quantitatively from the small expected OMR response for this geometry and the origin could be a topic of a careful future study. Considering that the magnetic field lies perpendicular to the Néel vector, this will induce a canting in the direction of  $\mathbf{H}$ , reducing the component of  $\mathbf{n}$  parallel to  $\mu_s$  at high magnetic fields and may lead to this deviation [26].

Although the behavior of the SMR for a field along a single direction indicates that  $\mathbf{n}$  dominates the transport response, it does not exclude the possibility of  $\mathbf{m}$  playing a role as it has been reported to contribute strongly to the SMR in thin films of a canted antiferromagnet [13]. To identify the governing factor for the SMR, we therefore rotate  $\mathbf{H}$  in the  $xy$  plane through an angle  $\alpha$  [Fig. 1(e)]. Here, the longitudinal SMR response is calculated with respect to a field parallel to the charge current  $\Delta R_L = R_L - R_{\alpha=0^\circ}$  and normalized by the zero-field resistance of the device. In this plane, the SMR signal for both the longitudinal  $R_L$  and transverse  $R_T$  resistances shows a behavior that can be modeled by a  $\sin^2 \alpha$  relationship indicative of negative SMR and is thus dominated by the orientation of  $\mathbf{n}$ , even in the presence of the spontaneous net moment. The magnitude of the SMR response between the uniaxial measurements [Figs. 1(b) and 1(c)] which are relative to the zero-field resistance of the devices, and the angular-dependent longitudinal resistance in Fig. 1(e) which is determined as the change in the SMR between  $\mathbf{H} // x$  and  $\mathbf{H} // y$  are consistent with one another. Due to the existence of a magnetic domain structure in the absence of a magnetic field in our films (see Supplemental Material [22]), the SMR response of antiferromagnets cannot be unambiguously resolved from angular-dependent measurements below the critical magnetic fields alone.

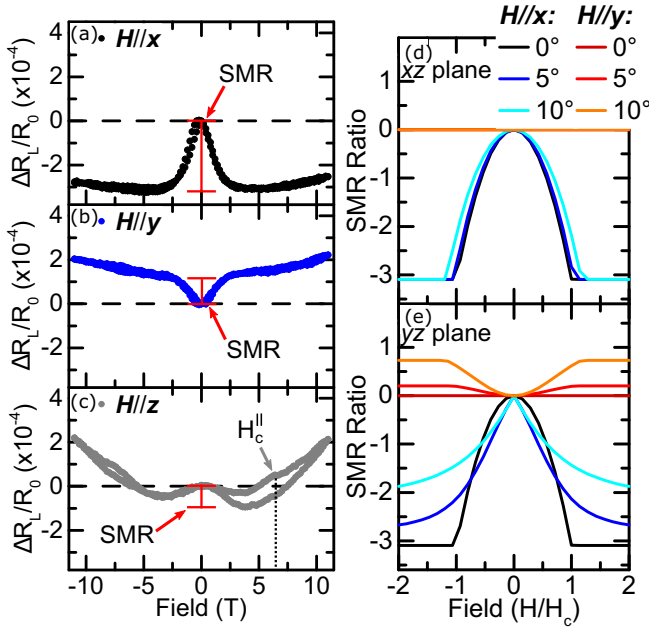


FIG. 2. Longitudinal resistance of Pt/hematite at 175 K in the easy-axis phase for a magnetic field applied along the (a)  $x$  axis (b)  $y$  axis, and (c)  $z$  axis.  $\Delta R_L = R_L - R_0$ , where  $R_0$  is the zero-field resistance. Error bars where visible represent the standard deviation of the data point. We indicate in (c) the critical magnetic field  $H_c^{\parallel}$  for an increasing magnetic field. (d), (e) Expected effect on the SMR ratio for a misalignment of the easy axis in the  $xz$  plane (d) or the  $yz$  plane (e) for a magnetic field applied in plane along either  $x$  or  $y$ . The critical field of the magnetic field induced second-order transition of the Néel vector is  $H_c = (2JK_z - D^2)/D$ , where  $J$  is the strength of the exchange interaction,  $K_z$  is the uniaxial anisotropy, and  $D$  is the strength of the antisymmetric exchange interaction (DMI). This transition describes a rotation of the Néel vector to a state perpendicular to both the easy axis and the magnetic field.

Next we check the effect of the antiferromagnetic symmetries, for which the surface sensitive nature of SMR is well suited [10,26]. Below  $T_M$ , the antiferromagnetic structure has an EA structure and  $\mathbf{n}$  lies along the  $z$  axis. For  $\mathbf{H} \perp \text{EA}$  ( $\mathbf{H} // x$  and  $\mathbf{H} // y$ ),  $\mathbf{n}$  undergoes a transition unique to hematite at some critical field  $H_c^{\perp}$  [33,34], smoothly rotating perpendicular to both the EA and  $\mathbf{H}$ . Considering first the case for  $\mathbf{H} // x$ ,  $\mathbf{n}$  rotates and the final state above  $H_c^{\perp}$  is that of  $\mathbf{n} // y$ , decreasing the expected SMR. Alternatively, we can apply  $\mathbf{H} // y$ , which also induces a rotation of  $\mathbf{n}$  in the plane parallel to  $J_C$  and the SMR ratio is expected to remain constant [17,35]. Finally,  $\mathbf{H} // z$  induces a spin flop at  $H_c^{\parallel}$  and  $\mathbf{n}$  reorients from  $z$  to lie within the  $xy$  plane [34].

We investigate the SMR at 175 K, below  $T_M$ , for different orientations of the magnetic field relative to  $J_C$ . Starting from  $\mathbf{H} // x$  in Fig. 2(a),  $R_L$  begins to decrease as expected until it reaches  $\mu_0 H_c^{\perp} = 2.5$  T and saturates at  $3 \times 10^{-4}$ , a higher amplitude than seen above  $T_M$ . As  $\mathbf{H}$  continues to increase, there are no further changes to the magnetic state. We then investigate the SMR for  $\mathbf{H} // y$  [Fig. 2(b)] where our expectation is to observe only the contributions unrelated to the hematite films. However, surprisingly we observe a significant increase of  $R_L$  up to the same magnetic field as  $\mathbf{H} // x$ , which

must then be related to the orientation of  $\mathbf{n}$ . Before we attempt to explain this signal, we briefly discuss  $\mathbf{H} // z$ , where the resistance begins to decrease with increasing magnetic field due to a small field misalignment and  $\mathbf{n}$  begins to rotate. There is a parabolic effect possibly from the OMR, which masks the smaller effect of the spin-flop field,  $\mu_0 H_c^{\parallel} = 6.5$  T indicated in Fig. 2(c) for the increasing magnetic field. As the magnetic field is lowered, a hysteretic field dependence appears, where the critical field is shifted slightly due to the additional, stabilizing magnetoelastic energy of the spin-flop state above  $H_c^{\parallel}$  leading to different values for the increasing and decreasing field branch [36]. There is an asymmetry in the size of the hysteresis for a negative and positive magnetic field, possibly due to an asymmetry in the magnetostriction of hematite when the magnetic field is not perfectly along the easy axis [36]. If a magnetic field is rotated in the  $xy$  plane through an angle  $\alpha$ , we again resolve a  $\sin^2 \alpha$  dependence characteristic of negative SMR, just as above  $T_M$  in Fig. 1(e), a feature that arises due to the antisymmetric exchange interaction that enables the rotation of  $\mathbf{n}$  at  $H_c^{\perp}$ .

To investigate the origin of the signal for  $\mathbf{H} // y$ , we note that, when we discuss the relative field directions, these are relative to the charge current of the Hall bar. Given the (0001) orientation of the crystal growth, the low-temperature AFM structure is expected to lead to an easy axis parallel to the geometric  $z$  axis (perpendicular to the film plane), which coincides with the (0001) axis of the  $\text{Al}_2\text{O}_3$  substrates. Measurements of the crystalline structure of our films by x-ray diffraction reveal a hematite peak with a full width at half maximum of  $0.538^{\circ} \pm 0.009^{\circ}$ , see Supplemental Material [22]. This is not unexpected given the 5% lattice mismatch between hematite and sapphire ( $5.038$  vs  $4.785$  Å) resulting in strained growth that relaxes as the films get thicker. However, this could also lead to a slight deviation of the hematite (0001) axis from the film normal (See Supplemental Material [22]). To investigate the effect that a small deviation from the geometric  $z$  axis has on the SMR response, we develop a simple model of hematite (see Supplemental Material [22]). Starting first from the naive assumption of the easy axis perfectly coincident with the out of plane direction, we reproduce the expected response for  $\mathbf{H} // x$  and  $\mathbf{H} // y$ . We then model the response as a function of angle for a deviation from  $z$  of the EA in both the  $xz$  plane and the  $yz$  plane. For a deviation in the  $yz$  plane, the impact on both field directions is profound, while the effect of a deviation in the  $xz$  plane is minimal. For a deviation between these two extremes, the effect on the SMR will similarly be between these two extremes. Comparing these theoretical expectations with our experimental results, it is clear that a small deviation of  $\mathbf{n}$  from the EA gives rise to the experimentally observed SMR response for  $\mathbf{H} // y$ . It is unlikely that the deviation in our films is confined to a single plane as it is for our calculations. Instead, it likely presents a range of deviations across the average of the Hall bar, and thus the SMR response is the average of all these deviations. To confirm that this model is quantitatively consistent with the thin-film magnetic structure, we performed x-ray magnetic linear dichroism-photoemission electron microscopy (XMLD-PEEM) imaging of the same thin-film samples used for the electrical measurements oriented as (0001) and compare the magnetic contrast to (1 $\bar{1}$ 02)-oriented films grown under the same conditions

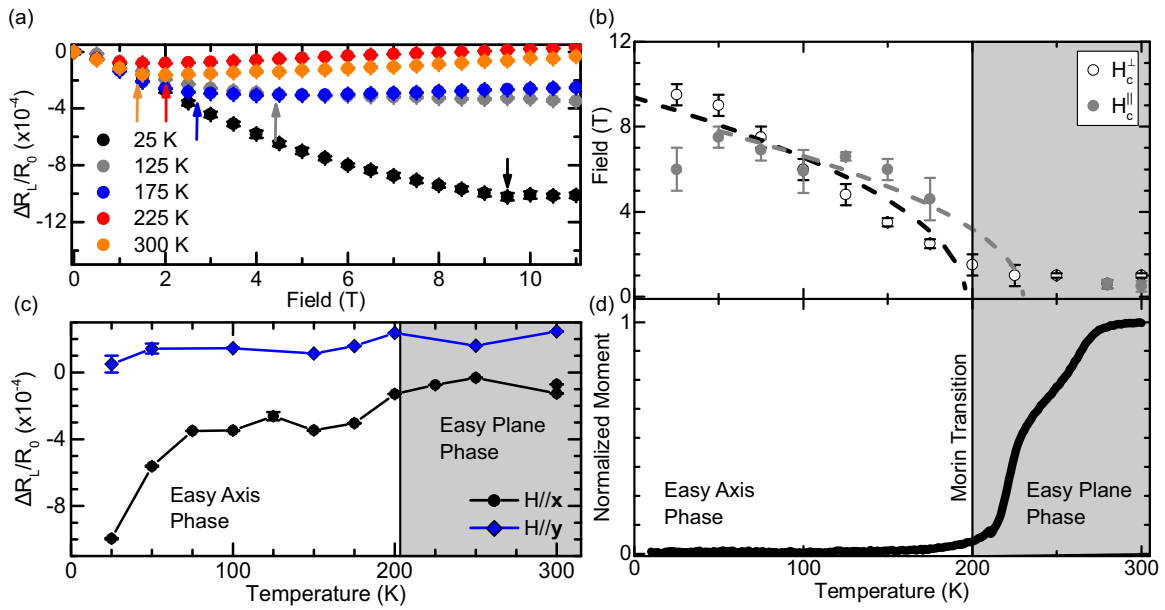


FIG. 3. (a) Temperature dependence of the normalized longitudinal resistance for a magnetic field  $H//x$ . The arrows indicate the critical magnetic field  $H_c^\perp$  for each temperature. (b) Temperature dependence of the critical fields for  $H//x$  ( $H_c^\parallel$ ) and  $H//z$  ( $H_c^\perp$ ). (c) Temperature dependence of the SMR ratio for  $H//x$  (black) and  $H//y$  (blue). (d) Normalized magnetic susceptibility of 100-nm-thick (0001)-orientated hematite for a field parallel to the  $c$  axis. The Morin transition is indicated.

(see Supplemental Material [22]). In the case of the (0001)-oriented films, we observe a magnetic contrast, which likely arises from a distribution in the  $c$ -axis directions of the films, even in the easy-axis phase, where the  $180^\circ$  nature of the AFM domains should lead to no contrast between them. However, the only impact of this domain structure on the SMR response is the emerging hysteresis in Fig. 2(c) (see Supplemental Material [22]). In single-crystal antiferromagnets, the domain structure is not considered [26] and we find here that the presence of large domains in thin films does not lead to an improved SMR response (see Supplemental Material [22]). Such an effect is not noticeable when measuring the SMR response of an easy-plane AFM given the nature of the anisotropy and that the SMR is sensitive to the net change of the projection  $\mathbf{n} \cdot \boldsymbol{\mu}_s$ . Only by moving to an easy-axis AFM can this lead to the anomalous signals observed here. Previous measurements of the SMR on the easy-axis AFM  $\text{Cr}_2\text{O}_3$  do not report similar effects [9,16]. However, for the (0001) growth orientation, this effect was only noticeable for  $H \perp \text{EA}$ , a configuration in  $\text{Cr}_2\text{O}_3$  that does not lead to a spin reorientation and thus does not affect the relative alignment of  $\mathbf{n}$ . We also note that we do not see a similar effect for (1 $\bar{1}$ 02)-oriented films, where the  $c$  axis of the hematite lies parallel to the substrate  $c$  axis and has a projection in plane (see Supplemental Material [22]).

Finally, we turn our attention to the temperature dependence of the SMR. In Fig. 3(a) the temperature dependence of the SMR for  $H//x$  at select temperatures is shown. The arrows indicate the critical field for rotation of  $\mathbf{n}$  at either  $H_c^\perp$  or  $H_{\text{MD}}$ . We extract the critical fields from the saturation point for  $H_c^\perp$  and plot it alongside the temperature dependence for  $H_c^\parallel$ , extracted from the SMR for  $H//z$ , in Fig. 3(b). With decreasing temperature, these fields increase, in line with bulk measurements of the critical fields [26,34]; however, to our knowledge, the temperature dependence of  $H_c^\perp$  for thin-film

hematite has not been reported. The strong temperature dependence of the magnetic anisotropies of hematite determine the critical fields  $H_c^\parallel$  and  $H_c^\perp$  as well as  $T_M$ , where they drop to zero [34]. The temperature dependence of the anisotropy is expected to scale by  $H_c \propto \sqrt{T_M - T}$  following a typical temperature dependence of a second-order Landau phase transition [26,28]. We then use this functional form to fit the critical fields of Fig. 3(b), indicated by the dashed lines, providing an estimate of  $T_M \sim 195 - 230$  K. Through the Morin transition, we see a low value of the SMR ratio for  $H//x$  [Fig. 3(c)] that decreases as we move away from the transition, the anisotropies begin to increase, and the thermal fluctuations of the transition are suppressed by the lowering temperature [8,28]. The spurious contribution for  $H//y$  [Fig. 3(c)] experiences a drop of 50% across the transition, before adopting a behavior that does not depend on the temperature. This drop across the transition can be explained by the absence of the SMR contribution from the domain redistribution at  $H_{\text{MD}}$  with the persistent contribution coming from the previously discussed tilt of the easy axis relative to the lab frame. The increase in the absolute value of the SMR ratio is contrary to the decrease with temperature observed in Ref. [32], attributed to anisotropic magnetoresistance (AMR). This contribution to the SMR was only visible for thin Pt layers 2 nm thick, while the OMR of thicker films masked this effect [32]. Given the thickness of our Pt (7 nm), alongside the increase with lower temperatures [Fig. 3(c)], any AMR contribution to our signal is likely to be negligible [32]. Using the data of Fig. 3(c), we can estimate a lower limit on the real part of the effective spin-mixing conductance  $G^{\uparrow\downarrow}$  for our Pt/ $\alpha$ - $\text{Fe}_2\text{O}_3$  in the two antiferromagnetic phases (see Supplemental Material [22]). Above the Morin transition in the easy-plane phase, we find  $G^{\uparrow\downarrow}$ , a value comparable to other easy-plane antiferromagnets [7]. At lower temperatures, we observe a change in the



value of  $G^{\uparrow\downarrow}$  from  $G^{\uparrow\downarrow} \sim 4.60 \times 10^{14} \Omega^{-1} \text{m}^{-2}$  just below the Morin transition to  $G^{\uparrow\downarrow} \sim 8.20 \times 10^{14} \Omega^{-1} \text{m}^{-2}$  at 25 K. Although the temperature dependence of  $G^{\uparrow\downarrow}$  is not clear [37–39], we find a continuous decrease of  $G^{\uparrow\downarrow}$  across the phase transition from easy plane to easy axis.

From superconducting quantum interference device (SQUID) magnetometry [see Supplemental Material [22] and Fig. 3(d)], the Morin transition of the 100-nm films used here can be measured in order to confirm the value of  $T_M$  from electrical measurements. If the films are thinner than this, the Morin transition is heavily suppressed or cannot be resolved [40]. We observe that, when cooled in an external field, the Morin transition of our films is visible from the drop in magnetic moment to effectively zero above the background substrate contributions [Fig. 3(d)]. The transition takes place over a relatively broad temperature range but below 200 K, the transition is complete and the films are in the purely easy-axis phase. The value of  $T_M$  given by SQUID is then comparable not only to synchrotron measurements on similar films [11] but also with the value extracted from our electrical measurements. We note that in other SMR studies on thinner films of hematite [32,41], the films have not demonstrated a Morin transition and remain in the easy-plane phase. It is then only by virtue of having a Morin transition are we able to observe the impact of the crystal growth. SQUID magnetometry can also be used to investigate the magnitude of  $H_c^{\parallel}$  and  $H_c^{\perp}$ ; however, thicker films are required in order to have sufficient signal to noise in the first derivative of the signal [42]. This further highlights the practicality of SMR in investigating the magnetic anisotropies of AFMs without the need for relying on volume effects.

In conclusion, the spin Hall magnetoresistance technique is shown to be an excellent tool for investigating antiferromagnets to understand the effects of anisotropies, symmetries, and surface symmetry breaking. The surface sensitivity nature of the technique allows for the extraction of the Morin transition even for thin films of hematite where conventionally used bulk-sensitive techniques fail. We find distinctly different behaviors above and below the Morin transition. By probing the SMR for different directions of the applied magnetic field, we observe an SMR response that cannot be described by assuming a perfect crystallographic orientation of the film. By considering the distribution of growth crystallites that accompanies thin-film deposition, we demonstrate that a small misalignment between the magnetic easy axis and the external geometric system can have large consequences for the SMR

response and the interpretation of the underlying magnetic symmetries. These conclusions are confirmed by direct imaging of the domain structure.

#### ACKNOWLEDGMENTS

A. Ross and M.K. acknowledge support from the Graduate School of Excellence Materials Science in Mainz (Grant No. DFG/GSC 266). This work was supported by the Max Planck Graduate Center with the Johannes Gutenberg-Universität Mainz (MPGC). A. Ross, R.L., and M.K. acknowledge support from the DFG Projects No. 423441604 and No. 403502522. R.L. acknowledges the European Union’s Horizon 2020 research and innovation programme under the Marie Skłodowska-Curie Grant Agreement FAST No. 752195. All authors from Mainz also acknowledge support from both MaHoJeRo (DAAD Spintronics network, Project No. 57334897), SPIN+X (DFG SFB TRR 173, Project No. A01) and KAUST (Grant No. OSR-2019-CRG8-4048.2). D.A.G., A.K., and A. Rothschild acknowledge support from the European Research Council under the European Union’s Seventh Framework programme (Grant No. FP/200702013)/ERC (Grant Agreement No. 617516). D.A.G. acknowledges support from The Center for Absorption in Science, Ministry of Immigrant Absorption, State of Israel. The work including the Mainz-Utrecht collaboration was also supported by the Research Council of Norway through its Centres of Excellence funding scheme, Project No. 262633 “QuSpin.” C.U. acknowledges support from the Nederlandse Organisatie voor Wetenschappelijk Onderzoek (NWO). L.B. acknowledges the European Union’s Horizon 2020 research and innovation programme under the Marie Skłodowska-Curie Grant Agreement ARTES No. 793159. Magnetic domain imaging measurements were carried out at the PEEM instrument of the UE49-PGMa beamline at Helmholtz-Zentrum Berlin für Materialien und Energie. We thankfully acknowledge the financial support from HZB under Proposal No. 182-07628 ST.

R.L. and M.K. proposed and supervised the project. A. Ross performed the transport experiments. A. Ross patterned the samples with R.L. D.G, A.K, and A. Rothschild grew and optimized the films. A. Ross and R.L. analyzed the data with input from M.K. C.U. developed the theoretical model with input from A. Ross. L.B., R.L., F.K. and S.V. performed the magnetic imaging and analysis. A. Ross wrote the paper with R.L., C.U. and M.K. All authors commented on the manuscript.

- 
- [1] V. Baltz, A. Manchon, M. Tsoi, T. Moriyama, T. Ono, and Y. Tserkovnyak, *Rev. Mod. Phys.* **90**, 015005 (2018).
  - [2] T. Jungwirth, J. Sinova, A. Manchon, X. Marti, J. Wunderlich, and C. Felser, *Nat. Phys.* **14**, 200 (2018).
  - [3] R. Lebrun, A. Ross, S. A. Bender, A. Qaiumzadeh, L. Baldrati, J. Cramer, A. Brataas, R. A. Duine, and M. Kläui, *Nature (London)* **561**, 222 (2018).
  - [4] J. Sinova, S. O. Valenzuela, J. Wunderlich, C. H. Back, and T. Jungwirth, *Rev. Mod. Phys.* **87**, 1213 (2015).
  - [5] Ø. Johansen, H. Skarsvåg, and A. Brataas, *Phys. Rev. B* **97**, 054423 (2018).
  - [6] J. Cramer, U. Ritzmann, B.-W. Dong, S. Jaiswal, Z. Qiu, E. Saitoh, U. Nowak, and M. Kläui, *J. Phys. D: Appl. Phys.* **51**, 144004 (2018).

- [7] L. Baldrati, A. Ross, T. Niizeki, C. Schneider, R. Ramos, J. Cramer, O. Gomonay, M. Filianina, T. Savchenko, D. Heinze, A. Kleibert, E. Saitoh, J. Sinova, and M. Kläui, *Phys. Rev. B* **98**, 024422 (2018).
- [8] G. R. Hoogeboom, A. Aqeel, T. Kuschel, T. T. M. Palstra, and B. J. van Wees, *Appl. Phys. Lett.* **111**, 052409 (2017).
- [9] Y. Ji, J. Miao, Y. M. Zhu, K. K. Meng, X. G. Xu, J. K. Chen, Y. Wu, and Y. Jiang, *Appl. Phys. Lett.* **112**, 232404 (2018).
- [10] K. Ganzhorn, J. Barker, R. Schlitz, B. A. Piot, K. Ollefs, F. Guillou, F. Wilhelm, A. Rogalev, M. Opel, M. Althammer, S. Geprägs, H. Huebl, R. Gross, G. E. W. Bauer, and S. T. B. Goennenwein, *Phys. Rev. B* **94**, 094401 (2016).
- [11] D. S. Ellis, E. Weschke, A. Kay, D. A. Grave, K. D. Malviya, H. Mor, F. M. F. de Groot, H. Dotan, and A. Rothschild, *Phys. Rev. B* **96**, 094426 (2017).
- [12] J. H. Han, C. Song, F. Li, Y. Y. Wang, G. Y. Wang, Q. H. Yang, and F. Pan, *Phys. Rev. B* **90**, 144431 (2014).
- [13] T. Hajiri, L. Baldrati, R. Lebrun, M. Filianina, A. Ross, N. Tanahashi, M. Kuroda, W. L. Gan, T. O. Mentş, F. Genuzio, A. Locatelli, H. Asano, and M. Kläui, *J. Phys.: Condens. Matter* **31**, 445804 (2019).
- [14] M. Isasa, S. Vélez, E. Sagasta, A. Bedoya-Pinto, N. Dix, F. Sánchez, L. E. Hueso, J. Fontcuberta, and F. Casanova, *Phys. Rev. Appl.* **6**, 034007 (2016).
- [15] Y. Ji, J. Miao, K. K. Meng, Z. Y. Ren, B. W. Dong, X. G. Xu, Y. Wu, and Y. Jiang, *Appl. Phys. Lett.* **110**, 262401 (2017).
- [16] R. Schlitz, T. Kosub, A. Thomas, S. Fabretti, K. Nielsch, D. Makarov, and S. T. B. Goennenwein, *Appl. Phys. Lett.* **112**, 132401 (2018).
- [17] Y.-T. Chen, S. Takahashi, H. Nakayama, M. Althammer, S. T. B. Goennenwein, E. Saitoh, and G. E. W. Bauer, *Phys. Rev. B* **87**, 144411 (2013).
- [18] F. J. Morin, *Phys. Rev.* **78**, 819 (1950).
- [19] D. A. Grave, H. Dotan, Y. Levy, Y. Piekner, B. Scherrer, K. D. Malviya, and A. Rothschild, *J. Mater. Chem. A* **4**, 3052 (2016).
- [20] T. J. Chuang, C. R. Brundle, and K. Wandelt, *Thin Solid Films* **53**, 19 (1978).
- [21] R. J. Lad and V. E. Henrich, *Surf. Sci.* **193**, 81 (1988).
- [22] See Supplemental Material at <http://link.aps.org/supplemental/10.1103/PhysRevB.102.094415> for x-ray-diffraction and magnetometry measurements, details on the theoretical model and the calculation of the effective spin-mixing conductance, transport measurements on (1 $\bar{1}$ 02)-oriented hematite, and magnetic imaging, which includes Ref. [43].
- [23] K. P. Belov, A. K. Zvezdin, A. M. Kadomtseva, and R. Z. Levitin, *Sov. Phys.-Usp.* **19**, 574 (1976).
- [24] G. Cinader, *Phys. Rev.* **155**, 453 (1967).
- [25] P. R. Elliston and G. J. Troup, *J. Phys. C: Solid State Phys.* **1**, 169 (1968).
- [26] R. Lebrun, A. Ross, O. Gomonay, S. A. Bender, L. Baldrati, F. Kronast, A. Qaiumzadeh, J. Sinova, A. Brataas, R. A. Duine, and M. Kläui, *Commun. Phys.* **2**, 50 (2019).
- [27] H. Gomonay and V. M. Loktev, *J. Phys.: Condens. Matter* **14**, 3959 (2002).
- [28] P. J. Besser, A. H. Morrish, and C. W. Searle, *Phys. Rev.* **153**, 632 (1967).
- [29] A. Ross, R. Lebrun, O. Gomonay, D. A. Grave, A. Kay, L. Baldrati, S. Becker, A. Qaiumzadeh, C. Ulloa, G. Jakob, F. Kronast, J. Sinova, R. Duine, A. Brataas, A. Rothschild, and M. Kläui, *Nano Lett.* **20**, 306 (2020).
- [30] J. Fischer, O. Gomonay, R. Schlitz, K. Ganzhorn, N. Vlietstra, M. Althammer, H. Huebl, M. Opel, R. Gross, S. T. B. Goennenwein, and S. Geprägs, *Phys. Rev. B* **97**, 014417 (2018).
- [31] A. Manchon, *Phys. Status Solidi - Rapid Res. Lett.* **11**, 1600409 (2017).
- [32] Y. Cheng, S. Yu, A. S. Ahmed, M. Zhu, Y. Rao, M. Ghazisaeidi, J. Hwang, and F. Yang, *Phys. Rev. B* **100**, 220408(R) (2019).
- [33] V. I. Ozhogin and V. G. Shapiro, *JETP Lett.* **6**, 7 (1967).
- [34] B. R. Morrison, A. H. Morrish, and G. J. Troup, *Phys. Status Solidi* **56**, 183 (1973).
- [35] H. Nakayama, M. Althammer, Y.-T. Chen, K. Uchida, Y. Kajiwara, D. Kikuchi, T. Ohtani, S. Geprägs, M. Opel, S. Takahashi, R. Gross, G. E. W. Bauer, S. T. B. Goennenwein, and E. Saitoh, *Phys. Rev. Lett.* **110**, 206601 (2013).
- [36] R. Z. Levitin, A. S. Pakhomov, and V. A. Shchurov, *Zh. Eksp. Teor. Fiz.* **56**, 1242 (1969) [*Sov. Phys. J. Exp. Theor. Phys.* **29**, 669 (1969)].
- [37] S. Wang, L. Zou, X. Zhang, J. Cai, S. Wang, B. Shen, and J. Sun, *Nanoscale* **7**, 17812 (2015).
- [38] S. Meyer, M. Althammer, S. Geprägs, M. Opel, R. Gross, and S. T. B. Goennenwein, *Appl. Phys. Lett.* **104**, 242411 (2014).
- [39] S. R. Marmion, M. Ali, M. McLaren, D. A. Williams, and B. J. Hickey, *Phys. Rev. B* **89**, 220404(R) (2014).
- [40] F. F. H. Aragón, J. D. Ardisson, J. C. R. Aquino, I. Gonzalez, W. A. A. Macedo, J. A. H. Coaquira, J. Mantilla, S. W. da Silva, and P. C. Morais, *Thin Solid Films* **607**, 50 (2016).
- [41] J. Fischer, M. Althammer, N. Vlietstra, H. Huebl, S. T. B. Goennenwein, R. Gross, S. Geprägs, and M. Opel, *Phys. Rev. Appl.* **13**, 014019 (2020).
- [42] S. P. Pati, M. Al-Mahdawi, S. Ye, T. Nozaki, and M. Sashiki, *Phys. Status Solidi - Rapid Res. Lett.* **11**, 1700101 (2017).
- [43] L. Shen, J. Xia, X. Zhang, M. Ezawa, O. A. Tretiakov, X. Liu, G. Zhao, and Y. Zhou, *Phys. Rev. Lett.* **124**, 037202 (2020).